Physics Letters B 772 (2017) 657–662

Contents lists available at ScienceDirect

Physics Letters B

www.elsevier.com/locate/physletb

Neutron–^{19}C scattering: Towards including realistic interactions

A. Deltuva

Institute of Theoretical Physics and Astronomy, Vilnius University, Saulėtekio al. 3, LT-10257 Vilnius, Lithuania

ARTICLE INFO

Article history:
Received 2 May 2017
Received in revised form 17 June 2017
Accepted 17 July 2017
Available online 21 July 2017
Editor: J.-P. Blaizot

Keywords:
Three-body scattering
Efimov physics
Faddeev equations
Pauli-forbidden states

ABSTRACT

Low-energy neutron–^{19}C scattering is studied in the three-body $n+n+{}^{18}$C model using a realistic nn potential and a number of shallow and deep n–^{18}C potentials, the latter supporting deeply-bound Pauli-forbidden states that are projected out. Exact Faddeev-type three-body scattering equations for transition operators including two- and three-body forces are solved in the momentum-space partial-wave framework. Phase shift, inelasticity parameter, and cross sections are calculated. For the elastic n–^{19}C scattering in the $J^\Pi = 0^+$ partial wave the signatures of the Efimov physics, i.e., the pole in the effective-range expansion and the elastic cross section minimum, are confirmed for both shallow and deep models, but with clear quantitative differences between them, indicating the importance of a proper treatment of deeply-bound Pauli-forbidden states. In contrast, the inelasticity parameter is mostly correlated with the asymptotic normalization coefficient of the ^{19}C bound state. Finally, in the regime of very weak ^{19}C binding and near-threshold (bound or virtual) excited ^{20}C state the standard Efimovian behaviour of the n–^{19}C scattering length and cross section was confirmed, resolving the discrepancies between earlier studies by other authors (Mazumdar et al., 2006 [20], Yamashita et al., 2007 [23]).

1. Introduction

Few-particle systems whose two-particle (ij) subsystems are characterized by large s-wave scattering lengths a_{ij} exhibit universal properties. Their systematic theoretical study was pioneered by V. Efimov almost 50 years ago [1] but the experimental confirmation came many years later [2–5]. It was achieved in cold-atom systems where the two-atom scattering length in the vicinity of the Feshbach resonance can be controlled by an external magnetic field and thereby tuned to a large value significantly exceeding the interaction range, a condition needed for the manifestation of the so-called universal or Efimov physics. The possibility of tuning the scattering length is not available in the nuclear physics. Nevertheless, some nuclear systems have quite large two-particle scattering lengths and qualitatively show some properties characteristic for Efimov physics. The simplest case is the three-nucleon system [1,6–11]. Further examples are systems consisting of a nuclear core (A) and two neutrons (n) provided that there is a weakly bound or virtual s-wave state in the $(A+n)$ subsystem [12–16]. Among them the $^{18}\mathrm{C}+n+n$ system has been studied in a number of works (see Refs. [15,16] for a review) hoping to establish the existence of a ^{20}C excited Efimov state assuming that ^{19}C has the binding energy of only $S_n = 0.16$ MeV [17] while the ground state of ^{20}C is bound with $S_{2n} = 3.5$ MeV (relative to the $^{18}\mathrm{C}+n+n$ threshold). However, more recent experiments have not confirmed such a weak binding of ^{19}C and presently accepted value is $S_n = 0.58(9)$ MeV [18], thereby excluding also the possibility of excited Efimov state in ^{20}C as a real bound state. Nevertheless, the $^{18}\mathrm{C}+n+n$ system in the low-energy $n+{}^{19}\mathrm{C}$ scattering process is expected to exhibit some universal properties that have been studied theoretically both in zero-range and finite-range models [19–22]. However, there is no consensus on the fate of the ^{20}C excited Efimov state as ^{19}C binding increases towards its physical value. Refs. [21–23] predict that it becomes a virtual state leading to a pole in the effective-range expansion for $n+{}^{19}\mathrm{C}$ scattering similar to the neutron–deuteron case [24] while Refs. [19,20,25] claim that the ^{20}C excited state turns into a continuum resonance seen as a pronounced peak in the $n+{}^{19}\mathrm{C}$ elastic cross section around 1.5 keV center-of-mass (c.m.) energy. One of the conclusions drawn in Ref. [25] was that "there is a need to undertake a detailed investigation using realistic interaction". Indeed, all the calculations for the $n+{}^{19}\mathrm{C}$ scattering so far have been performed using simple rank-one separable potentials with Yamaguchi form factors for n–n and n–^{18}C pairs. Although in the ideally universal regime the predictions for observables should be independent of the interaction details, some remnant dependence

E-mail address: arnoldas.deltuva@tfai.vu.lt.

http://dx.doi.org/10.1016/j.physletb.2017.07.036

is expected for realistic systems whose universal behaviour is modified by finite-range corrections.

The goal of the present work is to study the low-energy $n+{}^{19}$C scattering using more realistic interactions, possibly establishing shortcomings of rank-one separable models, and sort out the differences between findings of Refs. [19,20,25] and [21–23]. The improvement of the interaction models is threefold: (i) For the n–n pair a realistic high-precision charge-dependent (CD) Bonn potential [26] is used. (ii) A rank-one separable potential can support at most one bound state, thus, it misses deeply-bound core-neutron states. These states are occupied by internal neutrons in the core (not treated explicitly) and therefore are Pauli-forbidden and must be projected out. In this way the identity of external neutrons and those within the core is approximately taken into account. A proper treatment of Pauli-forbidden states was found to be important in scattering processes, see e.g. Ref. [27] for α–deuteron collisions. Using a n–^{18}C potential supporting the $2s$ state with the 0.58 MeV experimental value [18] of the ^{19}C binding energy and projecting out the deep $1s$ state will enable to study the importance of the Pauli-forbidden state for the $n+{}^{19}$C scattering and its impact on the Efimov physics. (iii) Depending on the chosen two-particle potentials, an additional three-body force (3BF) may be needed to fix the ^{20}C ground-state binding energy that must be included also in the $n+{}^{19}$C scattering calculations.

Thus, for the desired study of the $n+{}^{19}$C scattering an accurate theoretical description of three-particle scattering process including general form of potentials and 3BF is needed; the separable quasi-particle formulation of Refs. [19–22] is not applicable. In the present work the description is obtained by a combination and extension of momentum-space techniques from Refs. [27,28]. Both are based on exact Faddeev three-body theory [29] in the integral form for transition operators as proposed by Alt, Grassberger, and Sandhas (AGS) [30], but either neglecting the 3BF [27] or limited to the three-nucleon system [28].

The employed potentials are described in Sec. 2 and the three-body scattering equations with 3BF in Sec. 3. Results are presented in Sec. 4, and a summary is given in Sec. 5.

2. Potentials

The system of two neutrons and ^{18}C core is considered as a three-body problem. Particle masses $m_n = 1.00069\, m_N$ and $m_A = 18\, m_N$ are given in units of the average nucleon mass $m_N = 938.919$ MeV. The dynamics of the system is determined by two-particle potentials v_{nn} and v_{nA} acting within the nn pair and two nA pairs, and, eventually, by an additional 3BF. Unless explicitly stated otherwise, v_{nn} is taken to be the high-precision CD Bonn potential [26]; it is allowed to act in the s, p and d waves thereby ensuring a perfect convergence of the nn partial-wave expansion. Given the uncertainty in the v_{nA}, a number of models will be used. A very common choice is the Woods–Saxon potential, in the coordinate space defined as

$$\bar{v}_{nA}(r) = -V_c[1+\exp((r-R_v)/a_v)]^{-1}. \tag{1}$$

In the present work this kind of potentials is numerically transformed into the momentum-space representation and then used in two- and three-particle equations. The potentials parameters are the strength V_c, radius $R_v = r_v A^{1/3}$, and diffuseness a_v with standard values being around $r_v = 1.2$ fm and $a_v = 0.6$ fm; this parameter set is among the considered models. Two further models are taken as $r_v = 0.8$ fm and $r_v = 0.332$ fm keeping the ratio $a_v/r_v = 1/2$. In all three cases the strength V_c is adjusted such that the excited s-wave state $2s$ has the experimental ^{19}C binding energy value $\varepsilon_{2s} = S_n = 0.58$ MeV. The ground state is deeply bound with the energy ε_{1s} and the wave function $|\phi_{1s}\rangle$ depending on the chosen r_v, but it is Pauli-forbidden and therefore must be projected out. This is achieved [31,32,27] by taking the neutron-core s-wave potential as

Table 1
Parameters of the employed nA force models DPa, DPb, DPc and DPp with projected-out deeply-bound Pauli-forbidden states and 3BF. In the last line the parameters of the shallow WS potential are given.

	R_v (fm)	V_c (MeV)	Λ (fm^{-1})	W_c (fm^6 MeV)	ε_{1s} (MeV)
DPa	3.145	44.569	1.0	312.40	25.52
DPb	2.097	95.995	1.5	43.34	53.98
DPc	0.870	530.745		0.00	292.00
DPp	3.145	44.569	1.0	287.50	25.52
WS	3.119	8.317		0.00	0.58

$$v^s_{nA} = \bar{v}_{nA} + |\phi_{1s}\rangle\Gamma\langle\phi_{1s}| \tag{2}$$

where formally $\Gamma\to\infty$ but in practice Γ must be large enough such that the results for the three-body bound state(s) and scattering in the considered energy regime become independent of it; in the present work $\Gamma = 50$ GeV was proven to be sufficiently large. Simultaneously this ensures also the absence of deeply-bound three-body states. The potential models projecting out deeply-bound Pauli-forbidden (DP) states will be denoted as DPa, DPb, and DPc; their parameters are collected in Table 1. The predictions for the nA scattering length a_{nA} and the effective range r_{nA} are presented as well. As the potentials of Refs. [19–22], they are restricted to act in the s-wave only. The manifestation of the Efimov physics is governed by resonant s-wave interactions but in realistic systems also higher partial waves contribute. To estimate their effect, one more model, labeled DPp, is introduced that uses $\bar{v}_{nA}$ parameters from DPa but is allowed to act in p-waves as well. It turns out that $\bar{v}_{nA}$ supports a deeply-bound $1p$ state $|\phi_{1p}\rangle$ for ^{19}C with $\varepsilon_{1p} = 11.54$ MeV that is Pauli-forbidden as well and must be projected out in the same way, i.e.,

$$v^p_{nA} = \bar{v}_{nA} + |\phi_{1p}\rangle\Gamma\langle\phi_{1p}|. \tag{3}$$

Furthermore, as in Refs. [21,22] the energy of the three-body bound state, i.e., the two-neutron separation energy of ^{20}C, is fixed at its experimental value of $S_{2n} = 3.5$ MeV. Except for the DPc model whose range R_v was adjusted to reproduce S_{2n}, in general case the pairwise nn and nA interactions are insufficient for S_{2n} and an additional 3BF is needed. In fact, when the 3BF is not included, $S_{2n} = 2.083$, 2.404, and 2.126 MeV for DPa, DPb, and DPp, respectively. Being unable to derive the 3BF from a microscopic many-nucleon theory, usually a phenomenological form of the 3BF is assumed, depending either on the hyperradius [32] or hypermomentum [33,34]. The latter choice is obviously more convenient in the momentum-space framework and therefore is used in the present calculations. The three-body bound-state Faddeev equations, their solution technique, and the form of the 3BF is taken over from Ref. [34]. The latter is

$$\langle \mathbf{p}_\alpha \mathbf{q}_\alpha | W | \mathbf{p}'_\alpha \mathbf{q}'_\alpha \rangle = -(4\pi)^{-2} W_c\, g(\mathcal{K}^2) g(\mathcal{K}'^2) \tag{4}$$

with the hypermomentum $\mathcal{K}^2 = m_N(p^2_\alpha/\mu_\alpha + q^2_\alpha/M_\alpha)$ expressed in terms of Jacobi momenta $\mathbf{p}_\alpha$ for the pair and $\mathbf{q}_\alpha$ for the spectator and the associated reduced masses μ_α and M_α. Note that $\mathcal{K}^2/2m_N$ is the internal motion kinetic energy, thus, the 3BF has the same form in any Jacobi configuration labeled by the spectator particle α in the odd-man-out notation (see next section for more details). The form factor $g(\mathcal{K}^2) = \exp(-\mathcal{K}^2/2\Lambda^2)$ is chosen as a Gaussian. The cutoff parameter Λ is related to the interaction range R_W roughly as $\Lambda R_W \sim \sqrt{2}$; for each two-body model $R_W/R_v \sim \sqrt{2}/(\Lambda R_v) < 1/2$ ensuring that the 3BF is of shorter

Table 2
Predictions of the employed force models for the n–^{18}C scattering length a_{nA} and effective range r_{nA}, ANC of the ^{19}C nucleus, and the internal kinetic energy expectation value $\bar{K}_{3b}$ of the ^{20}C nucleus with the binding energy of $S_{2n} = 3.5$ MeV.

	a_{nA} (fm)	r_{nA} (fm)	ANC (fm$^{-1/2}$)	$\bar{K}_{3b}$ (MeV)
DPa	9.23	4.32	0.948	32.83
DPb	8.22	3.19	0.802	47.00
DPc	7.01	1.54	0.657	86.82
DPp	9.23	4.32	0.948	33.12
WS	8.12	3.04	0.792	9.87
Y	8.67	3.66	0.871	10.64
YY	8.68	3.67	0.872	11.14

range than v_{nA}. The strength W_c is adjusted to reproduce the desired three-body binding energy. These parameters are collected in Table 1 as well.

To isolate the effect of deeply-bound Pauli-forbidden states, several models without those states are used, i.e., they support only one ^{19}C bound state $1s$ with the binding energy $\varepsilon_{1s} = 0.58$ MeV. The model WS uses a shallow Woods–Saxon potential (1) with $r_v = 1.19$ fm, while the model labeled Y is a rank-one separable potential with Yamaguchi form factor as in Ref. [22] with the momentum-range parameter $\beta_{nc} = 0.6167\,\text{fm}^{-1}$. Finally, to get the insight on the importance of a realistic nn interaction, instead of the CD Bonn the rank-one separable nn potential with Yamaguchi form factor from Ref. [22] is used; its combination with the nA potential of the same type as Y but with $\beta_{nc} = 0.6131\,\text{fm}^{-1}$ will be labeled YY in the following. The above choices of the range parameter values for WS, Y, and YY models ensure the desired binding energy of ^{20}C without the 3BF. The WS, Y, and YY potentials will be referred in the following as *shallow*, in contrast to the *deep* ones DPa, DPb, DPc, and DPp.

To get an insight into the correlations between the interaction models and physical properties of ^{19}C and ^{20}C, in Table 2 the predictions for the n–^{18}C scattering length a_{nA} and effective range r_{nA}, the asymptotic normalization coefficient (ANC) of the ^{19}C bound state, and the ^{20}C ground state internal kinetic energy expectation value $\bar{K}_{3b}$ are collected. Within the group of deep models one may easily notice the well-known feature that a longer-range potential leads to larger values of the ANC, effective range, and, to a lesser extent, scattering length. However, comparing DPa and WS that have almost the same R, one can conclude that deeply-bound Pauli-forbidden states cause larger a_{nA}, r_{nA}, and ANC values, and significantly higher $\bar{K}_{3b}$. Within the group of DP models the kinetic energy expectation value depends also strongly on the range R, but in all cases it considerably exceeds the predictions of shallow potentials. Thus, deep potentials strongly enhance high-momentum components in the ^{20}C ground state.

3. Neutron–^{19}C scattering equations including 3BF

The momentum-space formulation of the three-body scattering theory is convenient when the underlying potentials have nonlocal terms such as those in the deep nA potentials projecting out Pauli-forbidden states. The present work is based on Faddeev equations for the multichannel transition operators $U_{\beta\alpha}$ in the version derived by Alt, Grassberger, and Sandhas (AGS) [30] but extended to include also the 3BF. Such extensions have been proposed in a number of works, e.g., [35,28], but their practical applications mostly were limited to the symmetrized version in the three-nucleon system. The general form of three-body equations from Ref. [28] is taken for the present study of the n–^{19}C scattering, i.e.,

$$\begin{aligned} U_{\beta\alpha} = {} & \bar{\delta}_{\beta\alpha} G_0^{-1} + u_\alpha + \sum_{\gamma=1}^{3} \bar{\delta}_{\beta\gamma} T_\gamma G_0 U_{\gamma\alpha} \\ & + \sum_{\gamma=1}^{3} u_\gamma G_0 (1 + T_\gamma G_0) U_{\gamma\alpha}, \end{aligned} \tag{5}$$

with $\bar{\delta}_{\beta\alpha} = 1 - \delta_{\beta\alpha}$, the free resolvent $G_0 = (E + i0 - H_0)^{-1}$ at the available energy E, the free Hamiltonian for the internal motion H_0, the two-body transition matrix

$$T_\gamma = v_\gamma + v_\gamma G_0 T_\gamma, \tag{6}$$

and the 3BF arbitrarily decomposed into three components

$$W = \sum_{\alpha=1}^{3} u_\alpha. \tag{7}$$

The odd-man-out notation is used, i.e., the channel α corresponds to the configuration where the particle α is the spectator and the remaining two are the pair. The decomposition of the 3BF into three symmetric parts (7) is essential for the symmetrization of three-nucleon equations [28] but is not needed in the present work. Labeling the particles n, A, n as 1, 2, 3 and taking $u_\alpha = \delta_{\alpha 2} W$, the system of the AGS equations (5) for the n–^{19}C scattering simplifies to

$$U_{\beta 1} = \bar{\delta}_{\beta 1} G_0^{-1} + \sum_{\gamma=1}^{3} \bar{\delta}_{\beta\gamma} T_\gamma G_0 U_{\gamma 1} + W G_0 (1 + T_2 G_0) U_{21} \tag{8}$$

with $\beta = 1, 2, 3$. The above system of integral equations is solved in the momentum-space partial-wave representation employing three sets of base functions $|p_\alpha q_\alpha (l_\alpha \{[L_\alpha (s_\beta s_\gamma) S_\alpha] j_\alpha s_\alpha\} \mathcal{S}_\alpha) J M\rangle$ with (α, β, γ) being cyclic permutations of $(1, 2, 3)$. Here p_α and q_α are magnitudes of Jacobi momenta for the corresponding pair and spectator, while L_α and l_α are the associated orbital angular momenta, respectively. Together with the particle spins s_α, s_β, s_γ they are coupled, through the intermediate subsystem spins S_α, j_α and $\mathcal{S}_\alpha$, to the total angular momentum J with the projection M. Only the basis $\alpha = 2$ is antisymmetric with respect to the permutation of the two neutrons; this is achieved by considering only even $L_2 + S_2$ states. However, the neutron identity is accounted for by taking the antisymmetrized elastic scattering amplitude

$$\begin{aligned} f_{\nu'\nu}(\mathbf{k}', \mathbf{k}) = {} & -(2\pi)^2 M_1 [\langle \Phi_1^{\nu'}(\mathbf{k}') | U_{11} | \Phi_1^{\nu}(\mathbf{k}) \rangle \\ & - \langle \Phi_3^{\nu'}(\mathbf{k}') | U_{31} | \Phi_1^{\nu}(\mathbf{k}) \rangle]. \end{aligned} \tag{9}$$

Here $|\Phi_\alpha^\nu(\mathbf{k})\rangle$ is the asymptotic state in the channel α; it is given by the product of the bound state wave function for the pair and the plane wave with the on-shell momentum $\mathbf{k}$ for the relative motion between the bound pair and spectator α satisfying $E = -S_n + k^2/2M_1$; the spin quantum numbers are abbreviated by ν. In the normalization of Eq. (9) the n–^{19}C elastic differential cross section for the $\nu\mathbf{k} \to \nu'\mathbf{k}'$ transition is simply $d\sigma/d\Omega = |f_{\nu'\nu}(\mathbf{k}', \mathbf{k})|^2$.

4. Results

The Efimov physics manifests itself in the states dominated by the s-wave components $L_\alpha = l_\alpha = 0$ for all α; this condition is satisfied only for $J^\Pi = 0^+$ where $\Pi = (-1)^{L_\alpha + l_\alpha}$ is the total parity. For the notational brevity suppressing the dependence on the on-shell momentum k, the S-matrix and the amplitude in the 0^+ state are parametrized as $s = e^{2i\delta}$ and $f = e^{i\delta} \sin\delta/k = (k \cot\delta - ik)^{-1}$, respectively. The phase shift δ is real below the inelastic threshold, i.e., at c.m. kinetic energies $E_k = k^2/2M_1 \le 0.58$ MeV, but becomes complex above this value due to the open breakup channel

Table 3
Parameters of the n–^{19}C effective-range expansion for the employed interaction models together with r_{nA} for n–^{18}C.

	a (fm)	b (fm^{-1} MeV^{-1})	c (fm^{-1} MeV^{-2})	E_0 (MeV)	r_{nA} (fm)
DPa	−6.299	1.176	−0.2726	0.20626	4.32
DPb	−6.103	1.078	−0.1538	0.26235	3.19
DPc	−5.369	1.033	−0.0511	0.33770	1.54
DPp	−6.310	1.176	−0.2744	0.20644	4.32
WS	−9.419	0.8194	−0.0496	0.39663	3.04
Y	−9.802	0.8520	−0.0838	0.34710	3.66
YY	−9.653	0.8591	−0.0828	0.34413	3.67

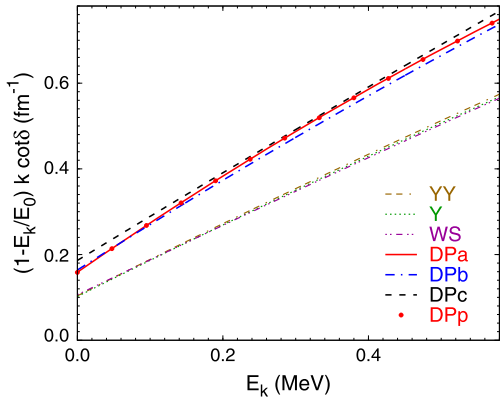

Fig. 1. (Color online.) n–^{19}C reduced effective-range functions $(1 - E_k/E_0)k\cot\delta$ in the $J^\Pi = 0^+$ partial wave for the interaction models YY (double-dashed–dotted), Y (dotted), WS (double-dotted–dashed), DPa (solid), DPb (dashed–dotted), DPc (dashed), and DPp (bullets).

whose importance is parametrized by the inelasticity parameter $\eta = |e^{2i\delta}| \le 1$.

The presence of the virtual Efimov state leads to a modified effective range expansion [24,22] containing a pole, i.e.,

$$k\cot\delta \approx \frac{-a^{-1} + bE_k + cE_k^2}{1 - E_k/E_0}, \tag{10}$$

where a is the n–^{19}C singlet scattering length and E_0 is the position of the pole. The values for the parameters a, b, c, and E_0 obtained fitting the n–^{19}C phase shift results at $E_k \le 0.58$ MeV for all employed interaction models are collected in Table 3 while the corresponding reduced effective-range functions $(1 - E_k/E_0)k\cot\delta$ are plotted in Fig. 1. It turns out that Eq. (10) yields a very good approximation – the quantities calculated directly and from the fitted parameters are indistinguishable in the plot. One notices immediately that $(1 - E_k/E_0)k\cot\delta$ predictions for the groups of the shallow (YY, Y, WS) and deep (DPa, DPb, DPc, DPp) potentials clearly separate. A closer inspection of the Table 3 reveals that this is mostly due to the differences in the n–^{19}C scattering length a and, to a lesser extent, in the parameter b. Within each group one can see qualitatively the same trend in correlations between the n–^{18}C effective range r_{nA} and n–^{19}C parameters, i.e., $|a|$, b and $|c|$ increase with increasing r_{nA} while E_0 decreases. However, it turns out that the presence of deep Pauli-forbidden states is more decisive for a and b than the correlation with r_{nA}, while for c and E_0 these two effects are of comparable importance. The parameters c and E_0 show a broad spread of values, especially in the group of deep potentials. However, if one disregards the DPc model as being of unrealistically short range, one can see again some trend, i.e., larger $|c|$ and smaller E_0 for deep potentials as compared to shallow ones. The parameters of DPa and DPp stay very close indicating that the n–^{18}C p-wave interaction is indeed irrelevant in the present context. The deviations between Y and YY for all parameters are insignificant as well, thus, the rank-one separable s-wave nn potential is able to capture relevant physics for the n–^{19}C low-energy $J^\Pi = 0^+$ elastic scattering.

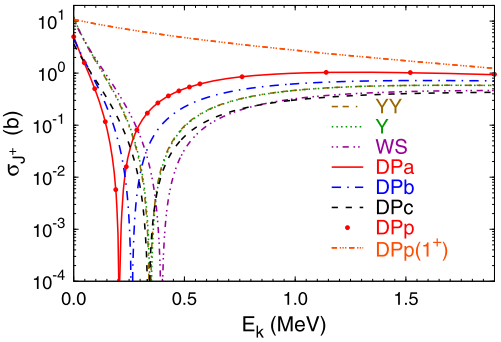

Fig. 2. (Color online.) n–^{19}C total elastic cross section σ_{0^+} in the $J^\Pi = 0^+$ partial wave as a function of the c.m. kinetic energy E_k for different interaction models. In addition, the $J^\Pi = 1^+$ wave cross section σ_{1^+} is shown for the DPp model as the upper triple-dotted–dashed curve, other curves are as in Fig. 1.

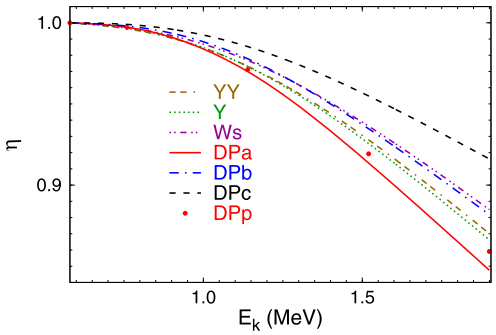

Fig. 3. (Color online.) n–^{19}C inelasticity parameter η in the $J^\Pi = 0^+$ partial wave as a function of the c.m. kinetic energy E_k for different interaction models. Curves are as in Fig. 1.

The differences in a and E_0 are clearly reflected in the $J^\Pi = 0^+$ total elastic cross section σ_{0^+} for the n–^{19}C scattering shown in Fig. 2: a determines σ_{0^+} at $E_k = 0$ while $E_k = E_0$ corresponds to the minimum of σ_{0^+}. However, this minimum is only clearly seen when the initial state n and ^{19}C spins are anti-parallel, such that the total channel spin $\mathcal{S}_1 = 0$ couples with $l_1 = 0$ to $J^\Pi = 0^+$. If the initial state is not polarized, one has to take into account also the n+^{19}C triplet state ($\mathcal{S}_1 = 1$, $l_1 = 0$) $J^\Pi = 1^+$ whose cross section σ_{1^+} is also shown in Fig. 2. In fact, σ_{1^+} yields by far the most sizable contribution to the unpolarized low-energy cross section, given (neglecting $l_1 = 1$ and higher waves) as the spin-weighted average $\sigma = (\sigma_{0^+} + 3\sigma_{1^+})/4$. Since the $^1S_0(nn)$ configuration is not allowed in the $J^\Pi = 1^+$ state, σ_{1^+} is governed by the nA interaction. In fact, for all models with the nn CD Bonn potential the n–^{19}C triplet scattering length $a_{1^+} \approx a_{nA} + 0.02$ fm is simply related to the n–^{18}C scattering length.

The results in Fig. 2 extend above the breakup threshold; in that regime σ_{0^+} depends on E_k only weakly, with the deep models (except for DPc) providing higher cross section than the shallow ones, although the spread within each group is comparable to the difference between groups. The DPa–DPp and Y–YY similarities remain valid also over the broader regime.

However, the situation is quite different for the inelasticity parameter η studied in Fig. 3. It exhibits some DPa–DPp and Y–YY deviations but shows no trend for the differences between shallow and deep potentials, the spread for the latter being very broad. Looking back to the model properties in Table 2, one may notice the correlations between the ANC (or a_{nA}, or r_{nA}) and η. To make it more evident, the inelasticity parameter at $E_k = 1.14$

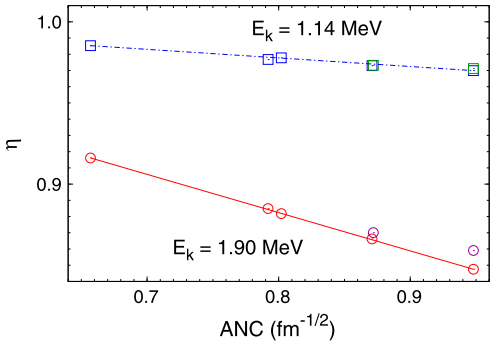

Fig. 4. (Color online.) n–^{19}C inelasticity parameter η in the $J^\Pi = 0^+$ partial wave at $E_k = 1.14$ (boxes) and 1.90 MeV (circles). The symbols from left to right correspond to the interaction models DPc, WS, DPb, YY, Y, DPa, and DPp. The lines are for guiding the eye only.

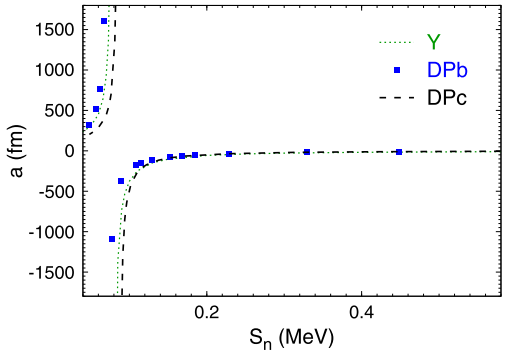

Fig. 5. (Color online.) Dependence of the n–^{19}C singlet scattering length a on the ^{19}C binding energy S_n for the evolved models Y (dotted), DPb (filled boxes) and DPc (dashed).

and 1.90 MeV for all force models is plotted in Fig. 4 against the corresponding ANC value. The dependence is roughly linear with deviations by YY and DPp models, that either have a different nn force (YY) from all the others, or have an additional nA p-wave dynamics (DPp). This is not surprising since one can expect the n–^{19}C breakup reaction to be peripheral at these low energies and dominated by the mechanism of the n–n knockout. In fact, even neglecting the 3BF for DPa, DPb and DPp models leads to changes of η that are significantly smaller than the spread of predictions in Fig. 3. Thus, the breakup and inelasticity parameter η is mostly governed by the properties of the ^{19}C bound state and the nn force, i.e., by the two-body physics without clear evidence for the three-body Efimov physics.

Finally I turn to the disagreement between Refs. [19,20,25] and [21–23] near the regime where the bound excited ^{20}C Efimov state disappears. To reach that regime the strength of the nA potential V_c is reduced without changes in other force parameters; this leads to the variations of ^{19}C and ^{20}C binding energies and n–^{19}C scattering observables. The appearance of the bound excited ^{20}C state, depending on the potential, takes place when S_n is reduced to 0.07–0.09 MeV and S_{2n} to 1.4–1.9 MeV. This is different from the strategy of Ref. [22] where S_{2n} was fixed at 3.5 MeV, but nevertheless the present results support the conclusions of Refs. [21, 22] that the excited ^{20}C state at the n+^{19}C threshold corresponds to a pole in the n–^{19}C scattering length, i.e., $a \to \pm\infty$, with $+(-)$ for S_n below (above) the critical value. This behaviour is shown in Fig. 5 for selected potential models, but is characteristic for all of them. In contrast, the authors of Refs. [19,20,25] claim that the n–^{19}C scattering length remains positive also for S_n above the critical value while the low-energy elastic n–^{19}C cross section exhibits a resonance around $E_k = 1.5$ keV on top of a nearly constant background. A thorough study of the n–^{19}C scattering in this regime performed in the present work excludes such a behaviour: the cross section rapidly and monotonically decreases with increasing energy without any signs of resonant peaks. As example the $J^\Pi = 0^+$ elastic cross section calculated using the evolved DPb model is shown in Fig. 6.

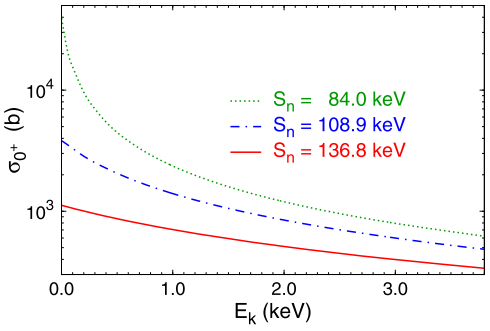

Fig. 6. (Color online.) n–^{19}C total elastic cross section σ_{0^+} in the $J^\Pi = 0^+$ partial wave as a function of the c.m. kinetic energy E_k for the DPb model evolved to have the ^{19}C binding energy S_n of 84.0 keV (dotted), 108.9 keV (dashed–dotted) and 136.8 keV (solid). The ^{20}C bound excited state exists below $S_n = 71.66$ keV.

5. Summary and conclusions

Low-energy neutron–^{19}C scattering was studied in the three-body ^{18}C+n+n model. Realistic nn CD Bonn potential and a number of shallow and deep n–^{18}C potentials of different range were used. All deep potentials support deeply-bound Pauli-forbidden states that were projected out thereby accounting for the identity of external neutrons and those within the ^{18}C core in an approximate way, while shallow models ignore this aspect. For all models the potential parameters were adjusted to reproduce the experimental binding of the ^{20}C ground state; most of the deep models had to be supplemented by a 3BF to achieve this goal. Exact three-body Faddeev-type scattering theory in the AGS version for transition operators, extended to include also the 3BF, was implemented in the momentum-space partial-wave framework yielding numerically accurate results for the n–^{19}C scattering both below and above breakup threshold.

Given the weak binding of ^{19}C and large nn scattering length, the ^{18}C + n + n system in the $J^\Pi = 0^+$ partial wave exhibits some features characteristic for Efimov physics. In particular, the presence of an excited ^{20}C Efimov state as a virtual state leads to a pole in the $J^\Pi = 0^+$ n–^{19}C effective range expansion. The reduced effective range functions $(1 - E_k/E_0)k\cot\delta$ clearly separate for shallow and deep models, indicating the importance of a proper treatment for deeply-bound Pauli-forbidden states. For some observables like the n–^{19}C singlet scattering length the presence of deep Pauli-forbidden states appears to be more decisive than the correlation with the n–^{18}C effective range. On the other hand, the observed differences between the groups of shallow and deep models are of comparable size as the finite range effects found in Ref. [22], and therefore do not invalidate the concept of the Efimov physics being independent of the short-range interaction details. However, the present work shows that deeply-bound Pauli-forbidden states may lead to systematic shifts within the limits of finite-range corrections. The effect is even more important for non-observable quantities like the expectation value of the ^{20}C internal kinetic energy.

For the elastic n–^{19}C scattering in the $J^\Pi = 0^+$ partial wave the signature of the Efimov physics, i.e., the presence of the cross section minimum, was confirmed for both shallow and deep models. It was also shown that without the initial antiparallel n–^{19}C polar-

ization this minimum is, however, hidden to a large extent due to the dominating contribution of the $J^\Pi = 1^+$ partial wave.

In the hypothetical situation of very weak ^{19}C binding and near-threshold (bound or virtual) excited ^{20}C state the standard Efimovian behaviour of the n–^{19}C scattering length and cross section was confirmed as well, clearly supporting Refs. [21–23] and excluding the possibility of near-threshold resonances predicted in Refs. [19,20,25]. As both groups have solved Faddeev equations with rank-one s-wave potentials, a possible explanation for this difference could be inaccurate numerical implementation in Refs. [19,20,25].

In contrast to the elastic n–^{19}C scattering, the breakup reaction is dominated by two-body physics. The inelasticity parameter in the $J^\Pi = 0^+$ partial wave is mostly correlated with the ANC of the ^{19}C bound state; this suggests a simple nn-knockout picture for the reaction mechanism.

Although the present work demonstrated the importance of the deeply-bound Pauli-forbidden states in the low-energy elastic n–^{19}C scattering, further changes can be expected given the low excitation energy of the ^{18}C core [18]. This would lead to the d-wave admixture in the ^{19}C ground state and possibly to d-wave excited states or resonances, thereby bringing d-wave corrections to the s-wave dominated Efimov physics of the $^{18}\mathrm{C}+n+n$ system. For example, significant d-wave effects have been found in the study of cold atom systems with van der Waals interactions [36].

This work was supported by Lietuvos Mokslo Taryba (Research Council of Lithuania) under Contract No. MIP-094/2015 and by Alexander von Humboldt-Stiftung under Contract No. LTU-1185721-HFST-E. The author acknowledges also the hospitality of the Ruhr-Universität Bochum where a part of this work was performed.

References

[1] V. Efimov, Phys. Lett. B 33 (1970) 563.
[2] T. Kraemer, et al., Nature 440 (2006) 315.
[3] S.E. Pollack, D. Dries, R.G. Hulet, Science 326 (2009) 1683.
[4] M. Zaccanti, B. Deissler, C. D'Errico, M. Fattori, M. Jona-Lasinio, S. Müller, G. Roati, M. Inguscio, G. Modugno, Nat. Phys. 5 (2009) 586.
[5] G. Barontini, C. Weber, F. Rabatti, J. Catani, G. Thalhammer, M. Inguscio, F. Minardi, Phys. Rev. Lett. 103 (2009) 043201.
[6] V. Efimov, Phys. Rev. C 44 (1991) 2303.
[7] P. Bedaque, U. van Kolck, Phys. Lett. B 428 (1998) 221.
[8] P. Bedaque, H.-W. Hammer, U. Van Kolck, Nucl. Phys. A 676 (2000) 357.
[9] P. Bedaque, G. Rupak, H. Grießhammer, H.-W. Hammer, Nucl. Phys. A 714 (2003) 589.
[10] S. König, H. Grießhammer, H.-W. Hammer, U. Van Kolck, J. Phys. G 43 (2016) 055106.
[11] A. Kievsky, M. Viviani, M. Gattobigio, L. Girlanda, Phys. Rev. C 95 (2017) 024001.
[12] A. Jensen, K. Riisager, D. Fedorov, E. Garrido, Rev. Mod. Phys. 76 (2004) 215.
[13] E. Braaten, H.-W. Hammer, Phys. Rep. 428 (2006) 259.
[14] H.-W. Hammer, L. Platter, Annu. Rev. Nucl. Part. Sci. 60 (2010) 207.
[15] T. Frederico, A. Delfino, L. Tomio, M. Yamashita, Prog. Part. Nucl. Phys. 67 (2012) 939.
[16] H.-W. Hammer, C. Ji, D. Philips, arXiv:1702.08605, 2017.
[17] G. Audi, A. Wapstra, C. Thibault, Nucl. Phys. A 729 (2003) 337.
[18] M. Wang, G. Audi, A. Wapstra, F. Kondev, M. MacCormick, X. Xu, B. Pfeiffer, Chin. Phys. C 36 (2012) 1603.
[19] V. Arora, I. Mazumdar, V.S. Bhasin, Phys. Rev. C 69 (2004) 061301.
[20] I. Mazumdar, A.R.P. Rau, V.S. Bhasin, Phys. Rev. Lett. 97 (2006) 062503.
[21] M. Yamashita, T. Frederico, L. Tomio, Phys. Lett. B 670 (2008) 49.
[22] M. Shalchi, M. Yamashita, M. Hadizadeh, T. Frederico, L. Tomio, Phys. Lett. B 764 (2017) 196;
M. Shalchi, M. Yamashita, M. Hadizadeh, T. Frederico, L. Tomio, Phys. Lett. B (2017), http://dx.doi.org/10.1016/j.physletb.2017.05.070, in press (Erratum).
[23] M.T. Yamashita, T. Frederico, L. Tomio, Phys. Rev. Lett. 99 (2007) 269201.
[24] W. van Oers, J. Seagrave, Phys. Lett. B 24 (1967) 562.
[25] I. Mazumdar, A.R.P. Rau, V.S. Bhasin, Phys. Rev. Lett. 99 (2007) 269202.
[26] R. Machleidt, Phys. Rev. C 63 (2001) 024001.
[27] A. Deltuva, Phys. Rev. C 74 (2006) 064001.
[28] A. Deltuva, Phys. Rev. C 80 (2009) 064002.
[29] L.D. Faddeev, Zh. Eksp. Teor. Fiz. 39 (1960) 1459, Sov. Phys. JETP 12 (1961) 1014.
[30] E.O. Alt, P. Grassberger, W. Sandhas, Nucl. Phys. B 2 (1967) 167.
[31] N.W. Schellingerhout, L.P. Kok, S.A. Coon, R.M. Adam, Phys. Rev. C 48 (1993) 2714.
[32] I.J. Thompson, B.V. Danilin, V.D. Efros, J.S. Vaagen, J.M. Bang, M.V. Zhukov, Phys. Rev. C 61 (2000) 024318.
[33] H.W. Hammer, L. Platter, Eur. Phys. J. A 32 (2007) 113.
[34] A. Deltuva, Phys. Rev. C 87 (2013) 034609.
[35] W. Glöckle, H. Witała, D. Hüber, H. Kamada, J. Golak, Phys. Rep. 274 (1996) 107.
[36] P.M.A. Mestrom, J. Wang, C.H. Greene, J.P. D'Incao, Phys. Rev. A 95 (2017) 032707.